Large optical spectral range dispersion engineered silicon-based photonic crystal waveguide modulator

Amir Hosseini,[1,3,*] Xiaochuan Xu,[2,3] Harish Subbaraman,[1,3] Che-Yun Lin,[2] Somayeh Rahimi,[2] and Ray T. Chen[2]

[1] *Omega Optics, Inc, 10306 Sausalito Dr, Austin, TX 78759, USA*
[2] *Microelectronics Research Center, Department of Electrical and Computer Engineering, University of Texas at Austin, 10100 Burnet Rd. Austin, TX 78758, USA*
[3] *Joint first authors*
[*] *amirh@utexas.edu*

Abstract: We present a dispersion engineered slow light silicon-based photonic crystal waveguide PIN modulator. Low-dispersion slow light transmission over 18nm bandwidth under the silica light line with a group index of 26.5 is experimentally confirmed. We investigate the variations of the modulator figure of merit, $V_\pi \times L$, as a function of the optical carrier wavelength over the bandwidth of the fundamental photonic crystal waveguide defect mode. A large signal operation with a record low maximum $V_\pi \times L$ of 0.0464 V·mm over the low-dispersion optical spectral range is demonstrated. We also report the device operation at 2GHz.

References and links

1. Y. A. Vlasov, M. O'Boyle, H. F. Hamann, and S. J. McNab, "Active control of slow light on a chip with photonic crystal waveguides," Nature **438**(7064), 65–69 (2005).
2. M. Soljačić, S. G. Johnson, S. Fan, M. Ibanescu, E. Ippen, and J. Joannopoulos, "Photonic-crystal slow-light enhancement of nonlinear phase sensitivity," J. Opt. Soc. Am. B **19**(9), 2052–2059 (2002).
3. R. Iliew, C. Etrich, T. Pertsch, and F. Lederer, "Slow-light enhanced collinear second-harmonic generation in two-dimensional photonic crystals," Phys. Rev. B **77**(11), 115124 (2008).
4. Y. Jiang, W. Jiang, L. Gu, X. Chen, and R. T. Chen, "80-micron interaction length silicon photonic crystal waveguide modulator," Appl. Phys. Lett. **87**(22), 221105 (2005).
5. M. Notomi, K. Yamada, A. Shinya, J. Takahashi, C. Takahashi, and I. Yokohama, "Extremely large group-velocity dispersion of line-defect waveguides in photonic crystal slabs," Phys. Rev. Lett. **87**(25), 253902 (2001).
6. H. C. Nguyen, Y. Sakai, M. Shinkawa, N. Ishikura, and T. Baba, "10 Gb/s operation of photonic crystal silicon optical modulators," Opt. Express **19**(14), 13000–13007 (2011).
7. H. Nguyen, Y. Sakai, M. Shinkawa, N. Ishikura, and T. Baba, "Photonic Crystal Silicon Optical Modulators: Carrier-Injection and Depletion at 10 Gb/s," IEEE J. Quantum Electron. **48**(2), 210–220 (2012).
8. J. H. Wülbern, J. Hampe, A. Petrov, M. Eich, J. Luo, A. K. Y. Jen, A. Di Falco, T. F. Krauss, and J. Bruns, "Electro-optic modulation in slotted resonant photonic crystal heterostructures," Appl. Phys. Lett. **94**(24), 241107 (2009).
9. J. M. Brosi, C. Koos, L. C. Andreani, M. Waldow, J. Leuthold, and W. Freude, "High-speed low-voltage electro-optic modulator with a polymer-infiltrated silicon photonic crystal waveguide," Opt. Express **16**(6), 4177–4191 (2008).
10. Y. Hamachi, S. Kubo, and T. Baba, "Slow light with low dispersion and nonlinear enhancement in a lattice-shifted photonic crystal waveguide," Opt. Lett. **34**(7), 1072–1074 (2009).
11. S. Schulz, L. O'Faolain, D. Beggs, T. White, A. Melloni, and T. Krauss, "Dispersion engineered slow light in photonic crystals: a comparison," J. Opt. **12**(10), 104004 (2010).
12. S. Rahimi, A. Hosseini, X. Xu, H. Subbaraman, and R. T. Chen, "Group-index independent coupling to band engineered SOI photonic crystal waveguide with large slow-down factor," Opt. Express **19**(22), 21832–21841 (2011).
13. L. O'Faolain, D. M. Beggs, T. P. White, T. Kampfrath, K. Kuipers, and T. F. Krauss, "Compact optical switches and modulators based on dispersion engineered photonic crystals," IEEE Photon. J. **2**(3), 404–414 (2010).
14. A. Mekis and J. Joannopoulos, "Tapered couplers for efficient interfacing between dielectric and photonic crystal waveguides," J. Lightwave Technol. **19**(6), 861–865 (2001).

15. C. Martijn de Sterke, K. B. Dossou, T. P. White, L. C. Botten, and R. C. McPhedran, "Efficient coupling into slow light photonic crystal waveguide without transition region: role of evanescent modes," Opt. Express **17**(20), 17338–17343 (2009).
16. A. Hosseini, X. Xu, D. N. Kwong, H. Subbaraman, W. Jiang, and R. T. Chen, "On the role of evanescent modes and group index tapering in slow light photonic crystal waveguide coupling efficiency," Appl. Phys. Lett. **98**(3), 031107 (2011).
17. C. H. Cox III, E. I. Ackerman, G. E. Betts, and J. L. Prince, "Limits on the performance of RF-over-fiber links and their impact on device design," IEEE Trans. Microw. Theory Tech. **54**(2), 906–920 (2006).
18. G. Li, C. Sun, S. Pappert, W. Chen, and P. Yu, "Ultrahigh-speed traveling-wave electroabsorption modulator-design and analysis," IEEE Trans. Microw. Theory Tech. **47**(7), 1177–1183 (1999).
19. C. Y. Lin, A. X. Wang, W. C. Lai, J. L. Covey, S. Chakravarty, and R. T. Chen, "Coupling loss minimization of slow light slotted photonic crystal waveguides using mode matching with continuous group index perturbation," Opt. Lett. **37**(2), 232–234 (2012).
20. L. Gu, W. Jiang, X. Chen, and R. T. Chen, "Physical mechanism of pin-diode-based photonic crystal silicon electrooptic modulators for gigahertz operation," IEEE J. Sel. Top. Quantum Electron. **14**(4), 1132–1139 (2008).
21. Y. Tang and B. Wang, "Study of active width-reduced line-defect photonic crystal waveguides for high speed applications," Proc. SPIE **7135**, 71350R, 71350R-8 (2008).
22. L. O'Faolain, S. A. Schulz, D. M. Beggs, T. P. White, M. Spasenović, L. Kuipers, F. Morichetti, A. Melloni, S. Mazoyer, J. P. Hugonin, P. Lalanne, and T. F. Krauss, "Loss engineered slow light waveguides," Opt. Express **18**(26), 27627–27638 (2010).
23. L. Gu, *Micro-and Nano-Periodic-Structure-Based Devices for Laser Beam Control 99–100* (ProQuest, 2007).

1. Introduction

Slow light in photonic crystal waveguides (PCWs) has been extensively studied for potential on-chip applications such as optical delay lines and enhanced non-linearity due to increased light-matter interaction [1-3]. Ultra-compact on-chip photonic devices can be realized by exploiting the enhanced light-matter interaction provided by the slow light operation [4]. However, the narrow optical bandwidth of non-engineered PCW slabs due to their highly dispersive group velocity in the slow light regime restricts their applications [5]. For example, a PCW Mach-Zehnder modulator operating with RF bandwidth as high as 10 Gb·s^{-1} was recently reported, with an optical wavelength range of only 0.7 nm [6-7]. Also, an electro-optic polymer refilled double heterostructure slotted PCW was shown to enable optical modulation over 0.7 nm optical wavelength range [8]. Therefore, in order to cover about 20 nm optical bandwidth in a typical integrated dense wavelength-division multiplexing (DWDM) system, several different designs will be necessary. In order to avoid having different PCW modulators for operation at each optical wavelength, a PCW modulator that can achieve slow light operation over a large bandwidth is required. A low-voltage and high speed optical modulator based on band-engineered slotted PCWs refilled with an electro-optic polymer was theoretically investigated in [9]. High-yield and repeatable low-dispersion slow-light devices can be achieved by fabrication-friendly dispersion engineering of PCWs with only a single hole size [10-12]. A band-engineered thermo-optic modulator with 10 nm optical wavelength range was demonstrated in [13]. Additionally, insertion of a group-index-taper coupler between the conventional strip waveguides and the low group velocity PCWs is necessary in order to efficiently couple light into and out of the device [14]. It was recently shown that due to the existence of the evanescent modes at the boundary between two photonic crystals with different group indices [15], short (8-16 periods) step-couplers can be used for efficient coupling between single mode silicon strip waveguides and low-dispersion slow light PCWs [16].

In optical interconnects, the link Noise Figure can be reduced by increasing the slope-efficiency of the modulation device without jeopardizing the bandwidth [17]. For a Mach–Zehnder modulator biased at quadrature, the slope efficiency is given as

$$s_{mzi} = \frac{dP_O}{di_m} = \frac{\pi P_I T_{ff} R_s}{2V_\pi} \tag{1}$$

where, P_o is the modulator's output optical power, i_m is the modulation input RF current, P_I is the laser power into the modulator, T_{ff} is the fiber-to-fiber transmission of the modulator, R_s is the impedance of the source, and V_π is the switching voltage of the modulator. Reducing the

switching voltage of the modulator, V_π, in order to enhance the slope-efficiency of the modulator is the most effective technique of reducing the effects of 1) the noise of the optical source, Relative Intensity Noise (RIN), 2) resistive thermal noise at the receiving end, and 3) the shot noise of the optical detector in the overall link Noise Fig [17]. It is also crucial to reduce the optical modulator length (L) to minimize the RC time constant for lumped electrode structure and the RF and optical signals velocity mismatch effect, as well as the RF loss for traveling wave electrode structure [18]. Overall, it is desirable to minimize the optical modulator $V_\pi \times L$ metric.

In this paper, we report a Mach Zehnder Interferometer (MZI) modulator based on a low-dispersion slow-light PCW with step couplers with the lowest $V_\pi \times L$ reported for a PCW based modulator to the best of our knowledge. We also investigate the variation of $V_\pi \times L$ as a function of the optical carrier wavelength, and experimentally confirm a low and nearly constant $V_\pi \times L$ over the low-dispersion slow light transmission region. Modulation operation up to 2 GHz is also experimentally confirmed using lumped electrodes.

2. Design and simulation

A schematic of the band engineered PCW is shown in Fig. 1(a). The lattice constant is a = 392 nm. The thickness of the silicon layer and the buried oxide layers are 250 nm and 3 µm, respectively. Refractive indices of the top cladding, core layer, and the bottom cladding materials are $n_{air} = 1$, $n_{Si} = 3.47$, $n_{SiO2} = 1.45$, respectively. Dispersion engineering is done by shifting the 3 innermost rows parallel to the defect line [12] with the parameters s_1, s_2, and s_3, as depicted in Fig. 1(a). Figure 2(b) shows the simulated band diagram for the dispersion engineered PCW with dW = 0, $s_1 = 0$, $s_2 = -0.05a$, $s_3 = 0.25a$, and r = 0.27a, where dW is the change in the width of the defect line with respect to a W1 PCW, and r is the hole radius. Variations of the group index (n_g) and group velocity dispersion (GVD) as functions of the wavelength are shown in Figs. 2(c) and 2(d), respectively. Group index $n_g = 26.7 \pm 10\%$ over a bandwidth of 18 nm (1539 nm~1557 nm), corresponding to delay–normalized bandwidth product of $n_g(\Delta\omega/\omega) = 0.31$, is achieved.
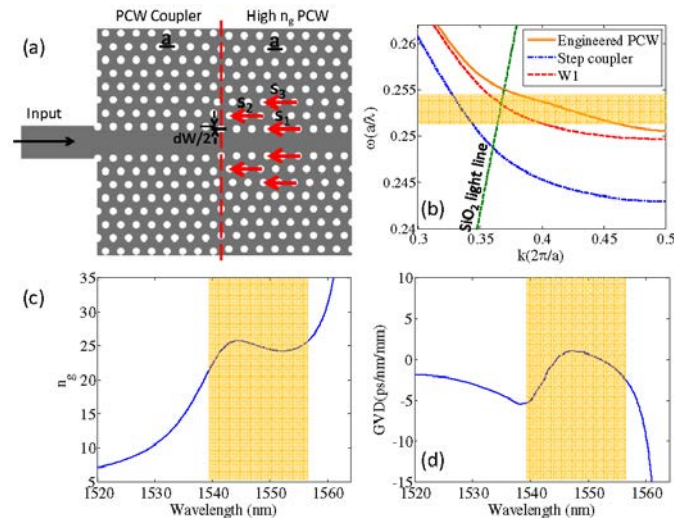
Fig. 1. (a) A schematic of band engineered PCW and PCW coupler. (b) Band structures of the designed band-engineered PCW and step PCW coupler. Silica light line (n = 1.45) is shown by a dashed green light. (c) Variations of the group index and (d) group velocity dispersion (GVD) over the bandwidth of intersect. (b), (c) and (d) are simulation results using 3D Rsoft Bandsolve. The low-dispersion slow-light wavelength range is highlighted in (b), (c) and (d).

In order to efficiently couple light into and out of the PCW from the input and output strip silicon waveguides, 8-period long PCW step couplers (dW = 0.15a, $s_1 = 0$, $s_2 = 0$, $s_3 = 0$, and r = 0.27a) are designed to interface the input and output strip waveguide to the slow light PCW

[12]. The band diagram of the PCW coupler is depicted in Fig. 1(b) that shows an overlap between the low-dispersion slow-light bandwidth of the engineered PCW and the low-dispersion fast-light bandwidth of the PCW coupler. Although the usable part of the band of the step coupler lies slightly above the silica light line, both numerical and experimental results show that the silica bottom cladding causes negligible radiation loss for a small number of periods (~<20) [16] [19].

In order to design a MZI modulator, one notices that utilizing the perturbation theory, the required length (L) of the MZI to achieve a π phase shift is given as [2]

$$\frac{L}{\lambda_0} \approx \frac{1}{2\sigma}\left(\frac{n}{\delta n}\right)\frac{1}{n_g} \qquad (2)$$

where, λ_0 is the free space wavelength, σ is the fraction of the total optical mode energy that propagates inside the region where the refractive index (n) is perturbed by an amount of δn. $n_g = c/v_g$ is the group index, where c and v_g are the speed of light and optical mode group velocity, respectively. Due to the high group index ($c/v_g > 25$) offered by our design, the length of the electrodes along the PCW can be short. We choose a length of 80 µm, in order to achieve π phase shift with low power operation, i.e. low δn change. In order to achieve the required refractive index perturbation, plasma dispersion effect in a PIN structure is utilized. A schematic of the structure in the active arm is shown in Fig. 2(a), and the doping profile is shown in Fig. 2(b).
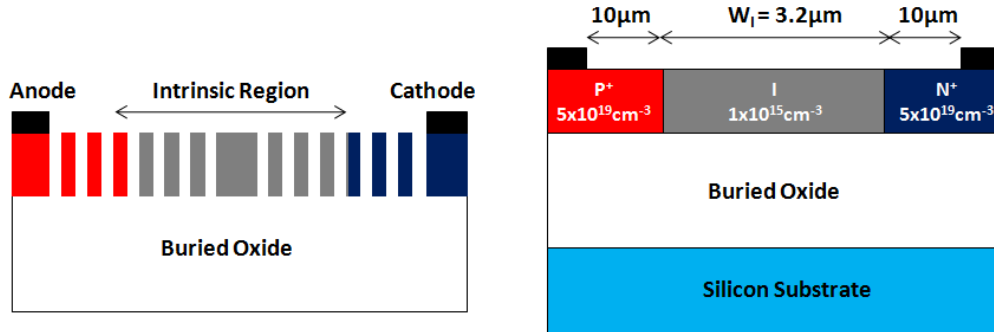
Fig. 2. Schematic of (a) PIN diode embedded PCW modulator arm, and (b) cross section showing doping concentrations and structural dimensions

In our previous demonstrations of PIN modulator, an intrinsic region width W_I of 4 µm was chosen and device operation up to 1 GHz was successfully demonstrated [4-16]. In order to push the operating speed beyond 1 GHz, and as a compromise between the switching speed and the propagation loss, for this work, we choose W_I of 3.2 µm [20-21].

Normally, the modal field profile changes drastically with wavelength near the band-edge [22] resulting in wavelength dependent σ. We notice a beneficial feature of the dispersion engineering, that is, constant group index over large optical bandwidth relatively distant from the band-edge. Therefore, we expect the PCW MZI to have similar characteristics (n_g and σ) over the entire low-dispersion slow light bandwidth.
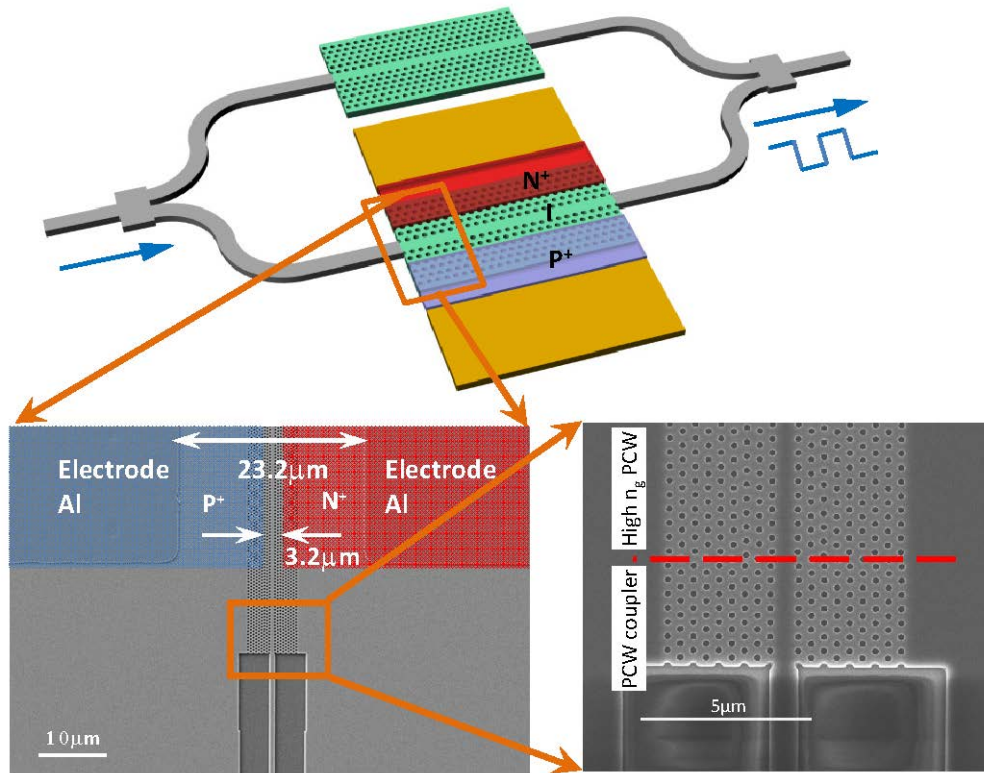
Fig. 3. A schematic of photonic crystal MZI modulator; scanning electronic microscope images of the active arm of the modulator and the photonic crystal waveguide coupler are shown as insets.

3. Fabrication

A symmetric MZI is designed by placing two 98 µm long PCWs (including 6.3 µm couplers) at the two arms. 1x2 Multimode Mode Interference couplers (MMIs) are used for beam splitting/combining, as shown in Fig. 3(a). One of the PCWs is doped to from a PIN, as shown in Fig. 3(b). The length of the electrodes is slightly less than that of the slow light PCWs to avoid break-down due to the generation of dense currents along the edges of PCWs, as discussed in [23].

The modulator is fabricated on a Uni-bond silicon-on-insulator wafer with a 250 nm top silicon layer and 3 µm buried oxide layer. Photonic crystal waveguides, photonic crystal couplers and strip waveguides are patterned in one step using a JEOL JBX-6000FS electron-beam lithography system followed by reactive ion etching. The windows for P^+ and N^+ implantation were opened by photolithography. Ion implantations of Boron at 30 KeV (surface concentration of $3.00 \times 10^{14}/cm^2$) and phosphorus at 50 KeV (surface concentration of $1.72 \times 10^{14}/cm^2$) were performed to obtain an average doping concentration of about 5×10^{19} cm^{-3}. Thermal rapid annealing for 1 min at 950 °C in a flowing nitrogen environment was performed afterwards to anneal the lattice defects and activate the implanted ions.

Electrode contact windows were then opened by photolithography and the native oxide inside the windows was removed. Aluminum electrodes were made by electron-beam evaporation and a subsequent lift off process. Finally, an ohmic contact was formed by post metallization annealing at a temperature of 400 °C for 30 mins [20]. SEM images of the fabricated PCW on one arm of the fabricated modulator device are also shown in Fig. 3.

4. Device characterization

The group index of a single PCW is determined through on-chip Fourier transform spectral interferometer, as previously reported [12]. Figure 4(a) shows the measured group index as a function of wavelength. Our results indicate a low-dispersion (with less than ± 10% fluctuations in group index) transmission over 18 nm bandwidth (1539 nm~1557 nm) with an average group index of 26.5. Figure 4(a) also shows the transmission characteristics of a single photonic crystal waveguide (including PCW couplers) obtained by coupling a Transverse Electric (TE)-polarized light from a broadband amplified spontaneous emission (ASE) source covering 1520~1620 nm into the Fourier transform spectral interferometer [12]. The transmission data is normalized to the output spectrum of a single mode waveguide. The insertion loss of a single PCW (excluding fiber-waveguide coupling losses and propagation loss inside silicon waveguides) is determined to be 3.8 ± 1.1 dB over the low dispersion bandwidth (1539 nm~1557 nm) [12].

The total insertion loss (fiber-to-fiber) is 19.8dB, which includes 7dB Fiber-to-strip waveguide coupling loss per facet, 3dB insertion loss for each MMI, and 3.8dB insertion loss for the PCW. From data mentioned above, one can see that the loss mainly comes from the fiber-to-waveguide coupling.

Before performing the modulation tests, we first performed static tests on the fabricated modulator devices. The static characteristic of the PIN diode obtained using Agilent B1500a semiconductor parameter analyzer is shown in Fig. 4(b). The forward linear resistance is ~200 Ohm.
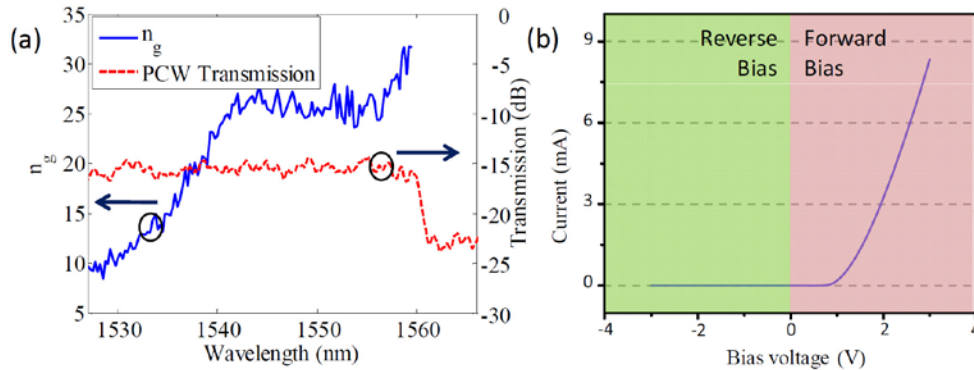
Fig. 4. (a) Output spectrum of PCW device (red curve) and the calculated group index based on FT method (blue curve). The PCW transmission curve is also provided as a reference; (b) static characteristic of the PIN diode;

Measurements of the figure of merit $V_\pi \times L$ and data transmission, described below, are carried out by coupling light from a TE-polarized tunable laser (Santec MLS-2000) into the device through butt coupling and tuning to $\lambda = 1550.48$ nm. The modulated output is detected with a gain switchable photodetector (Thorlab PDA10CS) and displayed on the oscilloscope (Agilent 86100A). The voltage V_π required to produce a carrier injection-induced π phase shift is measured by applying a 100 kHz triangular electrical drive signal, as shown in Fig. 5(a), to a MZI modulator with 80 μm long active arm under a forward bias $V_{bias} = 1.25$ V. The drive amplitude is increased until the slope of the modulated optical signal changed sign at the peaks/troughs of the drive waveform, as illustrated in Fig. 5(a) [6]. A complete half-period of optical modulation is observed for a peak-to-peak applied voltage of $V_\pi = 0.58$ V, leading to a figure of merit of $V_\pi \times L = 0.0464$ V·mm, which is less than one third of the lowest $V_\pi \times L$ for a PCW modulator reported so far [6].

Next, by tuning the optical carrier wavelength over the C band (1520 nm-1560 nm), we obtained variations of V_π versus optical wavelength as shown in Fig. 5(b). Due to Fabry-Perot oscillations caused by the input and output facets and also back reflections at the MMI's and

PCW's interfaces with the strip waveguides, the output optical power fluctuates with wavelength over the low-dispersion bandwidth. At wavelengths that correspond to the peaks of the Fabry-Perot oscillations, the output optical power is high and we are able to observe clear over-modulations [see Fig. 5(b)]. From the over-modulated signal, we were able to deduce the V_π value.

According to Eq. (2), at a constant L, since δn is linearly proportional to V_π, one can show

$$V_\pi \approx B \frac{\lambda_0}{n_g} \qquad (3)$$

where, B is a constant. The trend in V_π variations closely follow those of the group index as depicted in Fig. 4(a). Interestingly, the group index slightly increases at shorter wavelengths over the low-dispersion slow light bandwidth (λ≥1539nm); one notices that the V_π slightly decreases at shorter wavelengths over the low-dispersion slow light bandwidth consistent with Eq. (2) (λ≥1539nm).

The rectangular electrical signal for GHz operation is generated through Agilent 8133A 3 GHz pulse generator. The V_{bias} is 1.25 V and the V_{pp} is 1.50 V. The output optical signal is amplified by erbium-doped fiber amplifier and converted to electrical signal by a 22 GHz photodetector (DSC30S). The waveform is captured by Agilent 86100A as shown in Fig. 5(c). We were able to achieve 2 GHz operating speed using 80 μm long lumped electrodes. Due to excess noise generated by our EDFA, we were unable to accurately determine the extinction ratio of our modulator device.
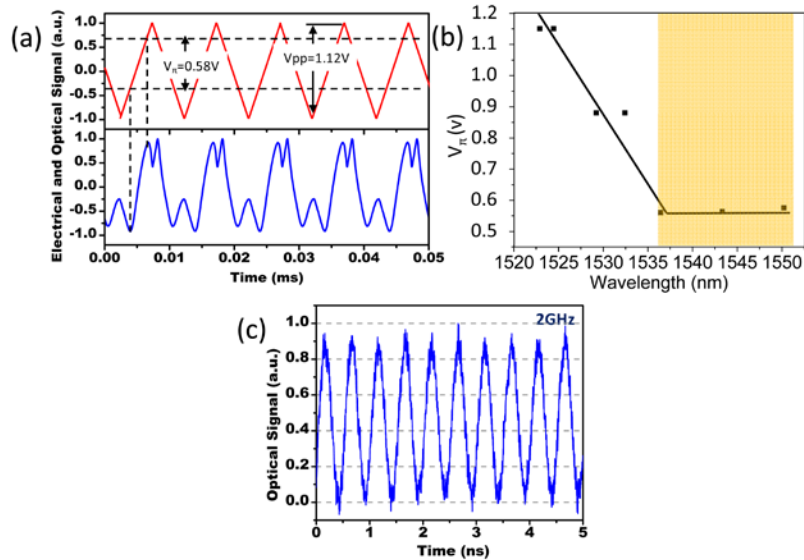
Fig. 5. (a) triangular electrical drive signal with a V_{pp} of 1.12 V and V_{offset} of 1.25 V (top). The over modulated optical signal indication a V_π of 0.58 V (bottom); (b) Variations of V_π versus the optical carrier wavelength; (c) the optical signal of 2 GHz operation at λ = 1550.48 nm. The low-dispersion slow-light wavelength range is highlighted in (b).

5. Conclusion

In conclusion, an ultra low-power, large bandwidth photonic-crystal-waveguide-based silicon Mach Zehnder modulator was proposed and demonstrated. The modulator arms consisted of

our designed band-engineered slow light photonic crystal waveguide, which demonstrated a large group index of 26.5 over an 18 nm bandwidth. By embedding the photonic crystal waveguide in a PIN diode structure, modulation operation with a record-low $V_\pi \times L$ of 0.0464 V.mm via carrier injection into an 80 µm long active section was experimentally demonstrated. The modulator $V_\pi \times L$ remains nearly constant over the low-dispersion slow-light bandwidth. Using the same structure, a maximum modulator operation up to 2GHz was also obtained. Further improvement in devices performance is expected by optimizing the electrical and optical design of the MZI structure.

Acknowledgments